

Joint Hierarchical Priors and Adaptive Spatial Resolution for Efficient Neural Image Compression

Ahmed Ghorbel Wassim Hamidouche Luce Morin

Abstract—Recently, the performance of neural image compression (NIC) has steadily improved thanks to the last line of study, reaching or outperforming state-of-the-art conventional codecs. Despite significant progress, current NIC methods still rely on ConvNet-based entropy coding, limited in modeling long-range dependencies due to their local connectivity and the increasing number of architectural biases and priors, resulting in complex underperforming models with high decoding latency. Motivated by the efficiency investigation of the Transformer-based transform coding framework, namely SwinT-ChARM, we propose to enhance the latter, as first, with a more straightforward yet effective Transformer-based channel-wise autoregressive prior model, resulting in an absolute image compression transformer (ICT). Through the proposed ICT, we can capture both global and local contexts from the latent representation and better parameterize the distribution of the quantized latents. Further, we leverage a learnable scaling module with a sandwich ConvNeXt-based pre-/post-processor to accurately extract more compact latent codes while reconstructing higher-quality images. Extensive experimental results on benchmark datasets showed that the proposed framework significantly improves the trade-off between coding efficiency and decoder complexity over the versatile video coding (VVC) reference encoder (VTM-18.0) and the neural codec SwinT-ChARM. Moreover, we provide model scaling studies to verify the computational efficiency of our approach and conduct several objective and subjective analyses to bring to the fore the performance gap between the adaptive image compression transformer (AICT) and the neural codec SwinT-ChARM. All materials, including the source code of AICT, will be made publicly accessible upon acceptance for reproducible research.

I. INTRODUCTION

Visual information is crucial in human development, communication, and engagement, and its compression is necessary for effective storage and transmission over constrained wireless and wireline channels. Thus, thinking about new enhanced lossy image compression solutions is a goldmine for scientific research. The goal is to reduce an image file size by permanently removing redundant data and less critical information, particularly high frequencies, to obtain the most compact bit-stream representation while preserving a certain level of visual fidelity. Despite this, optimizing the rate-distortion tradeoff involves a fundamental objective for achieving a high compression ratio and low distortion.

Conventional image and video compression standards, including JPEG [1], JPEG2000 [2], H.265/high-efficiency video coding (HEVC) [3], and H.266/versatile video coding

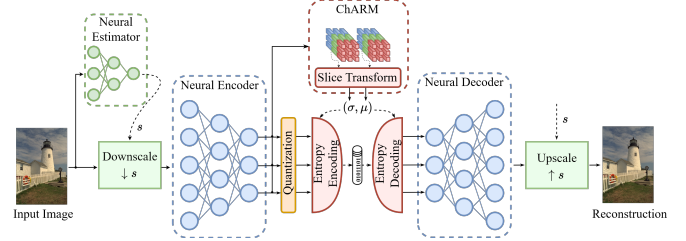


Fig. 1. A high-level diagram of the proposed AICT solution. ChARM refers to the Transformer-based channel-wise autoregressive prior model, and s represents the resizing parameter predicted by the neural estimator ($s \in \mathbb{R} \cap [0, 1]$).

(VVC) [4], rely on hand-crafted creativity within a block-based encoder/decoder diagram. In addition, these codecs employ intra-prediction, fixed transform matrices, quantization, context-adaptive arithmetic encoders, and various in-loop filters to reduce spatial and statistical redundancies and alleviate coding artifacts. However, it has taken several years to standardize a conventional codec. Moreover, existing image compression standards are not anticipated to be an ideal and global solution for all types of image content due to the rapid development of new image formats and the growth of high-resolution mobile devices.

On the other hand, with recent advancements in machine learning and artificial intelligence, new neural image compression (NIC) schemes [5] have emerged as a promising alternative to traditional compression methods. NIC consists of three modular parts: transform, quantization, and entropy coding. Each of these components can be represented as follows: i) autoencoders as flexible nonlinear transforms where the encoder (i.e., analysis transform) extracts a latent representation from an input image and the decoder (i.e., synthesis transform) reconstructs the image from the decoded latent ii) differentiable quantization that quantizes the encoded latent iii) deep prior model estimating the conditional probability distribution of the quantized latent to reduce the rate. Further, these three components are jointly optimized in end-to-end training by minimizing the distortion loss between the original image and its reconstruction, and the rate needed to transmit the bit-stream of latent representation.

Recently, we have seen a significant surge of deep learning-based lines of study exploring the potential of artificial neural networks (ANNs) to develop various NIC frameworks, reaching or even outperforming state-of-the-art conventional codecs. Some of these previous works leverage hyperprior-related side information [6], [7] to capture short-range spatial dependencies or additional context model [8], [9], and others

Ahmed Ghorbel and Luce Morin were with Univ. Rennes, INSA Rennes, CNRS, IETR - UMR 6164, Rennes, France, e-mail: (Ahmed.Ghorbel; Luce.Morin)@insa-rennes.fr.

Wassim Hamidouche was with Technology Innovation Institute, Masdar City, P.O Box 9639, Abu Dhabi, UAE, e-mail: Wassim.Hamidouche@tii.ae.

use non-local mechanism [10]–[13] to model long-range spatial dependencies. For example, Mentzer *et al.* [14] proposed a generative compression method achieving high-quality reconstructions. In contrast, Minnen *et al.* [15] introduced channel-conditioning and latent residual prediction taking advantage of an entropy-constrained model that uses both forward and backward adaptations. Current research trends has focused on attention-guided compressive transform, as Zhu *et al.* [16] replaced the ConvNet-based transform coding in the Minnen *et al.* [15] architecture with a Transformer-based nonlinear transform. Later, Zou *et al.* [17] combined the local-aware attention mechanism with the global-related feature learning and proposed a window-based attention module. An additional series of efforts have addressed new entropy coding methods, as Zhu *et al.* [18] proposed a probabilistic vector quantization with cascaded estimation to estimate pairs of mean and covariance under a multi-codebooks structure. Guo *et al.* [19] introduced the concept of separate entropy coding by dividing the latent representation into two channel groups, and proposed a causal context model that makes use of cross-channel redundancies to generate highly informative adjacent contexts. Further, Kim *et al.* [20] exploited the joint global and local hyperprior information in a content-dependent manner using an attention mechanism. He *et al.* [21] adopted stacked residual blocks as nonlinear transform and multi-dimension entropy estimation model. More recently, El-Nouby *et al.* [22] replaced the vanilla vector quantizer with product quantization (PQ) [23] in a compression system derived from vector-quantized variational autoencoder (VQ-VAE) [24] offering a large set of rate-distortion points and then introduced a novel masked image modeling (MIM) conditional entropy model that improves entropy coding by modeling the co-dependencies of the quantized latent codes. Further, Muckley *et al.* [25] introduced a new adversarial discriminator based on VQ-VAE that optimizes likelihood functions in the neighborhood of local images under the mean-scale hyperprior Minnen *et al.* [8] architecture. Other interesting attempts [26], [27], known as coordinate-based or implicit neural representations, have shown good ability to represent, generate, and manipulate various data types, particularly in NIC by training image-specific networks that map image coordinates to RGB values, and compressing the image-specific parameters. On the other hand, Wu *et al.* [28] proposed a learned block-based hybrid image compression method, which introduces a contextual prediction module to utilize the relationship between adjacent blocks, and propose a boundary-aware post-processing module to remove the block artifacts.

Through these numerous pioneering works, we can estimate the importance of NIC in the research field and the industry. Thus, identifying the main open challenges in this area is crucial. The first one is to discern the most relevant information necessary for the reconstruction, knowing that information overlooked during encoding is usually lost and unrecoverable for decoding. The second challenge is to enhance the trade-off between coding efficiency and decoding latency. While the existing approaches improve the transform and entropy coding accuracy, they still need to improve the decoding latency and reduce the model complexity, leading to an ineffective real-

world deployment. To tackle those challenges, we propose a nonlinear transform coding and channel-wise autoregressive entropy coding built on Swin Transformer [29] blocks and paired with a neural scaling network, namely adaptive image compression transformer (AICT). Fig. 1 portrays a high-level diagram to provide a more comprehensive overview of the proposed framework.

The contributions of this paper are summarized as follows:

- We propose the image compression transformer (ICT), a nonlinear transform coding and spatio-channel autoregressive entropy coding. These modules are based on Swin Transformer blocks for effective latent decorrelation and a more flexible receptive field to adapt to contexts requiring short/long-range information.
- We propose the AICT model that adopts a scale adaptation module as a sandwich processor to enhance compression efficiency. This module consists of a neural scaling network, and ConvNeXt-based [30] pre-/post-processor to optimize differentiable resizing layers jointly with a content-dependent resize factor estimator.
- We conduct extensive experiments on four widely-used benchmark datasets to explore possible coding gain sources and demonstrate the effectiveness of AICT. In addition, we carried out a model scaling analysis and an ablation study to substantiate our architectural decisions.

The experimental results reveal the impact of the spatio-channel entropy coding, the sandwich scale adaptation component, and the joint global structure and local texture learned by the attention units through the nonlinear transform coding. These experiments show that the proposed ICT and AICT achieve respectively -4.65% and -5.11% BD-rate (PSNR) reduction over VTM-18.0 while considerably reducing the decoding latency, outperforming conventional and neural codecs in the trade-off between coding efficiency and decoding complexity.

The rest of this paper is organized as follows. First, Section II briefly describes the background and related works. Then, Section III presents our overall framework along with a detailed description of the proposed architecture. Further, we devote Section IV to present and analyze the experimental results. Finally, Section V concludes the paper.

II. BACKGROUND AND RELATED WORKS

Over the past years, research has renewed interest in modeling image compression as a learning problem, giving a series of pioneering works [6]–[10], [15], [31]–[33] that have contributed to a universal fashion effect, and have achieved great success, augmented by the efficient connection to variational learning [34]–[36]. In the early stage, some of these methods adopted ConvNets and activation layers coupled with generalized divisive normalization (GDN) layers to perform non-linear transform coding over a variational autoencoder (VAE) architecture. This framework creates a compact representation of the image by encoding them to a latent representation. The compressive transform squeezes out the redundancy in the image with dimensional reduction and entropy constraints. Following that, some studies focus

on developing network architectures that extract compact and efficient latent representation while providing higher-quality image reconstruction.

This section reviews relevant NIC techniques, including works related to our research, while focusing on the following aspects. First, we briefly present the autoregressive context related works. Then, we describe the end-to-end NIC methods that have recently emerged, including attention-guided and Transformer-based coding. Finally, we introduce adaptive downsampling within the context of neural coding.

A. Autoregressive Context

Following the success of autoregressive priors in probabilistic generative models, Minnen *et al.* [8] was the first to introduce autoregressive and hierarchical priors within the variational image compression framework, featuring a mean-scale hyperprior. An additional context model is added to boost the rate-distortion performance. Although the combined model demonstrated superior rate-distortion performance compared to neural codecs, it came with a notable computational cost. Later, Cheng *et al.* [10] proposed the first model achieving competitive coding performance with VVC, using a context model in an autoregressive manner. They improved the entropy model by using a discretized K-component gaussian mixture model (GMM). In addition, Minnen *et al.* [15] estimated the latent distribution's mean and standard deviation in a channel-wise manner and incorporated an autoregressive context model to condition the already-decoded latent slices and the latent rounding residual on the hyperprior to further reduce the spatial redundancy between adjacent pixels. Finally, He *et al.* [37] proposed a parallelizable spatial context model based on the checkerboard-shaped convolution that allows parallel-friendly decoding implementation, thus increasing the decoding speed.

B. Attention-Guided Coding

Attention mechanism was popularized in natural language processing (NLP) [38], [39]. It can be described as a mapping strategy that queries a set of key-value pairs to an output. For example, Vaswani *et al.* [39] have proposed multi-headed attention (MHA) methods in which machine translation is frequently used. For low-level vision tasks [32], [40], [41], spatially adaptive feature activation is made possible by the attention mechanism, focusing on more complex areas, like rich textures, saliency, etc. In image compression, quantized attention masks are used for adaptive bit allocation, e.g., Li *et al.* [32] used a trimmed convolutional network to predict the conditional probability of quantized codes, Mentzer *et al.* [40] relied on a 3D-convolution neural network (CNN)-based context model to learn a conditional probability model of the latent distribution. Later, Cheng *et al.* [10] inserted a simplified attention module (without the non-local block) into the analysis and synthesis transforms to pay more attention to complex regions. More recently, Zou *et al.* [17] combined the local-aware attention mechanism with the global-related feature learning within an effective window-based local attention block, which can be used as a specific component to enhance ConvNet and Transformer models. Guo *et al.* [19] adopted

a powerful group-separated attention module to strengthen the non-linear transform networks. Further, Tang *et al.* [42] integrated graph attention and asymmetric convolutional neural network (acnn) for end-to-end image compression, to effectively capture long-range dependencies and emphasize local key features, while ensuring efficient information flow and reasonable bit allocation.

C. Transformer-based Coding

Recently, Transformers have been increasingly used in neural codecs. They exempt convolution operators entirely and rely on attention mechanisms to capture the interactions between inputs, regardless of their relative position, thus allowing the network to focus more on pertinent input data elements. Qian *et al.* [43] replaced the autoregressive hyperprior [8] with a self-attention stack and introduced a novel Transformer-based entropy model, where the Transformer's self-attention is used to relate different positions of a single latent for computing the latent representation. Zhu *et al.* [16] replaced all convolutions in the standard approach [6], [15] with Swin Transformer [29] blocks, leading to a more flexible receptive field to adapt tasks requiring both short/long-range information, and better progressive decoding of latent. Apart from their effective window-based local attention block, Zou *et al.* [17] proposed a novel symmetrical Transformer (STF) framework with absolute Transformer blocks for transform coding combined with a channel-wise autoregressive model (ChARM) prior. Inspired by the adaptive characteristics of the Transformers, Koyuncu *et al.* [44] proposed a Transformer-based context model, which generalizes the de facto standard attention mechanism to spatio-channel attention.

D. Adaptive Downsampling

Learning sampling techniques were first developed for image classification to improve image-level prediction while minimizing computation costs. Spatial transformer networks (STNs) [45] introduced a layer that estimates a parametrized affine, projective, and splines transformation from an input image to recover data distortions and thereby improve image classification accuracy. Recasens *et al.* [46] suggested that when downsampling an input image for classification, salient regions should be "zoomed-in" to learn a saliency-based network jointly. Talebi *et al.* [47] jointly optimize pixel value interpolated at each fixed downsampling location for classification. Marin *et al.* [48] recently argued that a better downsampling scheme should sample pixels more densely near object boundaries, and introduced a strategy that adapts the sampling locations based on the output of a separate edge-detection model. Further, Jin *et al.* [49] introduced a deformation module and a learnable downsampling operation, which can be optimized with the given segmentation model in an end-to-end fashion.

In the context of NIC, Chen *et al.* [50] proposed a straight-forward learned downsampling module that can be jointly optimized with any NIC kernels in an end-to-end fashion. Based on the STN [45], a learned resize parameter is used in a bilinear warping layer to generate a sampling grid, where

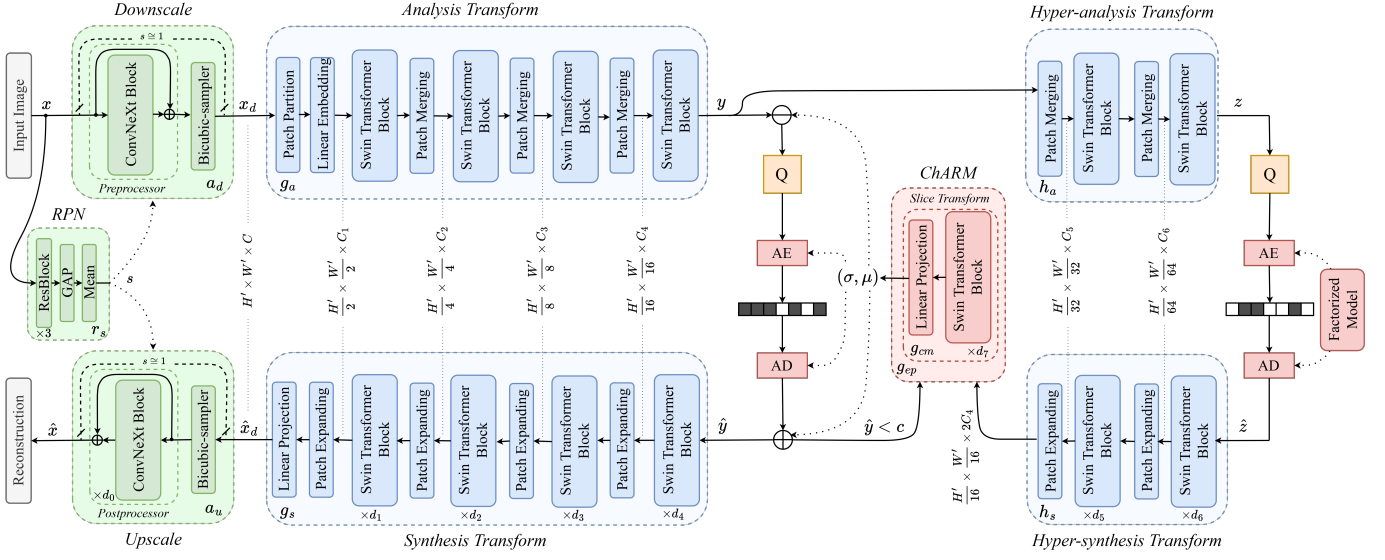


Fig. 2. Overall AICT Framework. We illustrate the image compression diagram of our AICT with hyperprior and Swin Transformer based ChARM, and scale adaptation module. The RPN, ConvNeXt block, and Swin Transformer block architectures are respectively detailed in (a), (c), and (d) Fig. 3.

the input should be sampled to produce the resampled output. They also include an additional warping layer necessary for an inverse transformation to maintain the same resolution as the input image.

III. PROPOSED AICT FRAMEWORK

In this section, we first formulate the NIC problem. Next, we introduce the design methodology for the overall AICT architecture, followed by the description of each component individually.

A. Problem Formulation

The primary challenges addressed in this work are twofold. Firstly, we aim to identify and prioritize the most pertinent information required for accurate reconstruction. It is crucial to acknowledge that any information overlooked during the encoding phase is typically lost and irretrievable during decoding. Secondly, we endeavor to optimize the delicate balance between coding efficiency and decoding latency. While existing approaches have made strides in improving the accuracy of transform and entropy coding, there remains a pressing need to mitigate decoding latency and streamline model complexity for practical real-world deployment. To tackle these challenges, we introduce a novel approach, denoted as AICT. AICT leverages nonlinear transform coding and channel-wise autoregressive entropy coding techniques, building upon Swin Transformer blocks and incorporating a neural scaling network. In the context of describing these contributions, it is imperative to establish a clear problem formulation, which we delve into in the following section. The objective of NIC is to minimize the distortion between the original image and its reconstruction under a specific distortion-controlling hyperparameter. For an input image x , the analysis transform g_a , with parameter ϕ_g ,

removes the image spatial redundancies and generates the latent representation y . Then, this latent is quantized to the discrete code \hat{y} using the quantization operator $\lceil \cdot \rceil$, from which a synthesis transform g_s , with parameter θ_g , reconstructs the image denoted by \hat{x} . The overall process can be formulated as follows:

$$\begin{aligned} y &= g_a(x \mid \phi_g), \\ \hat{y} &= \lceil y \rceil, \\ \hat{x} &= g_s(\hat{y} \mid \theta_g). \end{aligned} \quad (1)$$

A hyperprior model composed of a hyper-analysis and hyper-synthesis transforms (h_a, h_s) with parameters (ϕ_h, θ_h) is usually used to reduce the statistical redundancy among latent variables. In particular, this hyperprior model assigns a few extra bits as side information to transmit some spatial structure information and helps to learn an accurate entropy model. The generated hyper-latent representation z is quantized to the discrete code \hat{z} using the quantization operator $\lceil \cdot \rceil$. The hyperprior generation can be summarized as follows:

$$\begin{aligned} z &= h_a(y \mid \phi_h), \\ \hat{z} &= \lceil z \rceil, \\ p_{\hat{y}|\hat{z}}(\hat{y} \mid \hat{z}) &\leftarrow h_s(\hat{z} \mid \theta_h). \end{aligned} \quad (2)$$

Further, considering a context model g_{cm} with parameter ψ_{cm} , and a parameter inference network g_{ep} with parameter ψ_{ep} which estimates, from the latent \hat{y} , the location and scale parameters $\Phi = (\mu, \sigma)$ of the entropy model. The parameter prediction for i -th representation \hat{y}_i is expressed as follows:

$$\Phi_i = g_{ep}(h_s(\hat{z}), g_{cm}(\hat{y}_{<i} \mid \psi_{cm}) \mid \psi_{ep}), \quad (3)$$

where $\Phi_i = (\mu_i, \sigma_i)$ is used to jointly predict entropy parameters, and $\hat{y}_{<i} = \{\hat{y}_1, \dots, \hat{y}_{i-1}\}$ is the observable neighbors

of each symbol vector $\hat{\mathbf{y}}_i$ at the i -th location.

$$p_{\hat{\mathbf{y}}_i|\hat{\mathbf{z}}}(\hat{\mathbf{y}}_i | \hat{\mathbf{z}}) = \sum_{0 < k < K} \pi_i^k [\mathcal{N}_{(\mu_i^k, \sigma_i^{2k})} * \mathcal{U}_{(-\frac{1}{2}, \frac{1}{2})}](\hat{\mathbf{y}}_i), \quad (4)$$

where K groups of entropy parameters (π^k, μ^k, σ^k) are calculated by g_{ep} , $\mathcal{N}_{(\mu, \sigma^2)}$ represents the mean and scale Gaussian distribution, and $\mathcal{U}_{(-\frac{1}{2}, \frac{1}{2})}$ denotes the uniform noise.

Both transform and quantization introduce distortion $D = MSE(\mathbf{x}, \hat{\mathbf{x}})$ for mean squared error (MSE) optimization that measures the reconstruction quality with an estimated bitrate R , corresponding to the expected rate of the quantized latent and hyper-latent, as described below:

$$R = \mathbb{E} [-\log_2(p_{\hat{\mathbf{y}}|\hat{\mathbf{z}}}(\hat{\mathbf{y}} | \hat{\mathbf{z}})) - \log_2(p_{\hat{\mathbf{z}}}(\hat{\mathbf{z}}))]. \quad (5)$$

In the case of adaptive resolution (i.e., AICT), we consider the RPN, the downscale, and the upscale modules as (r_s, a_d, a_u) with parameters $(\omega_r, \omega_d, \omega_u)$, respectively. The generation process of \mathbf{x}_d and $\hat{\mathbf{x}}$ is described as follows:

$$\begin{aligned} s &= r_s(\mathbf{x} | \omega_r), \\ \mathbf{x}_d &= a_d(\mathbf{x}, s | \omega_d), \\ \hat{\mathbf{x}} &= a_u(\hat{\mathbf{x}}_d, s | \omega_u). \end{aligned} \quad (6)$$

Representing (g_a, g_s) , (h_a, h_s) , (g_{cm}, g_{ep}) , and (r_s, a_d, a_u) by deep neural networks (DNNs) enables jointly optimizing the end-to-end model by minimizing the rate-distortion trade-off \mathcal{L} , giving a rate-controlling hyperparameter λ . This optimization problem can be expressed as follows:

$$\begin{aligned} \arg \min \mathcal{L}(\mathbf{x}, \hat{\mathbf{x}}) &= \arg \min D(\mathbf{x}, \hat{\mathbf{x}}) + \lambda R, \\ &= \arg \min \|\mathbf{x} - \hat{\mathbf{x}}\|_2^2 + \lambda \underbrace{(\mathbb{H}(\hat{\mathbf{y}}) + \mathbb{H}(\hat{\mathbf{z}}))}_R, \end{aligned} \quad (7)$$

where \mathbb{H} stands for the cross entropy.

Finally, we recall that training the model with the gradient descent method requires substituting the quantization with additive uniform noise [51], preventing the gradient from vanishing at the quantization. We follow this method in this paper, where the noisy representations of the latent are used to compute the rate during the training phase.

B. Overall Architecture

The overall pipeline of the proposed solution is illustrated in Fig. 2. The framework includes three modular parts. First, the scale adaptation module, composed of a tiny resize parameter network (RPN) [50], a ConvNeXt-based pre/post-processor, and a bicubic interpolation filter. Second, the analysis/synthesis transform (g_a, g_s) of our design consists of a combination of patch merging/expanding layers and Swin Transformer [29] blocks. The architectures of hyper-transforms (h_a, h_s) are similar to (g_a, g_s) with different stages and configurations. Then, a Transformer-based slice transform inside a ChARM is used to estimate the distribution parameters of the quantized latent. Finally, the resulting discrete-valued data $(\hat{\mathbf{y}}, \hat{\mathbf{z}})$ are encoded into bit-streams with an arithmetic encoder.

C. Scale Adaptation Module

Given a source image $\mathbf{x} \in \mathbb{R}^{H \times W \times C}$, we first determine an adaptive spatial resize factor $s \in \mathbb{R} \cap [0, 1]$ estimated by the RPN module, which consists of three stages of residual blocks (ResBlocks). Indeed, the estimated resize parameter s is used to create a sampling grid τ_M following the convention STNs, and used to adaptively down-scale \mathbf{x} into $\mathbf{x}_d \in \mathbb{R}^{H' \times W' \times C}$ through the bicubic interpolation, with $H' = sH$ and $W' = sW$. The latter (i.e., \mathbf{x}_d) is then encoded and decoded with the proposed ICT. Finally, the decoded image $\hat{\mathbf{x}}_d \in \mathbb{R}^{H' \times W' \times C}$ is up-scaled to the original resolution $\hat{\mathbf{x}} \in \mathbb{R}^{H \times W \times C}$ using the same, initially estimated, resize parameter s . The parameterization of each layer is detailed in the RPN and ResBlock diagrams of Fig. 3 (a) and (b), respectively. In addition, a learnable depth-wise pre-/post-processor is placed before/after the bicubic sampler to mitigate the information loss introduced by down/up-scaling, allowing the retention of information. This neural pre-/post-processing method consists of concatenation between the input and the output of three successive ConvNeXt [30] blocks, using depth-wise convolutions with large kernel sizes to obtain efficient receptive fields. Globally, the ConvNeXt block incorporates a series of architectural choices from a Swin Transformer while maintaining the network's simplicity as a standard ConvNet without introducing any attention-based module. These design decisions can be summarized as follows: macro design, ResNeXt's grouped convolution, inverted bottleneck, large kernel size, and various layer-wise micro designs [30]. In Fig. 3 (c), we illustrate the ConvNeXt block, where the DConv2D(.) refers to the depthwise 2D convolution, LayerNorm for the layer normalization, Dense(.) for the densely-connected neural network layer, and gaussian error linear unit (GELU) for the activation function. Finally, it is essential to note that we propose to skip the scale adaptation module for a better complexity-efficient design when the predicted scale does not change the input resolution, i.e., $s \cong 1$. The overhead to store and transmit the scale parameter s can be ignored, given the large bitstream size of the image.

D. Transformer-based Analysis/Synthesis Transform

The analysis transform g_a contains four stages of patch merging layer and Swin Transformer block to obtain a more compact low-dimensional latent representation \mathbf{y} . In order to consciously and subtly balance the importance of feature compression through the end-to-end learning framework, we used two additional stages of patch merging layer and Swin Transformer block in the hyper-analysis transform to produce the hyperprior latent representation \mathbf{z} . During training, both latents \mathbf{y} and \mathbf{z} are quantized using a rounding function to produce $\hat{\mathbf{y}}$ and $\hat{\mathbf{z}}$, respectively. During inference, both latents \mathbf{y} and \mathbf{z} are first quantized using the same rounding function as training and then compressed using probability tables. The quantized latent variables $\hat{\mathbf{y}}$ and $\hat{\mathbf{z}}$ are then entropy coded regarding an indexed entropy model for a location-scale family of random variables parameterized by the output of the ChARM, and a batched entropy model for continuous random variables, respectively, to obtain the bit-streams. Finally, quan-

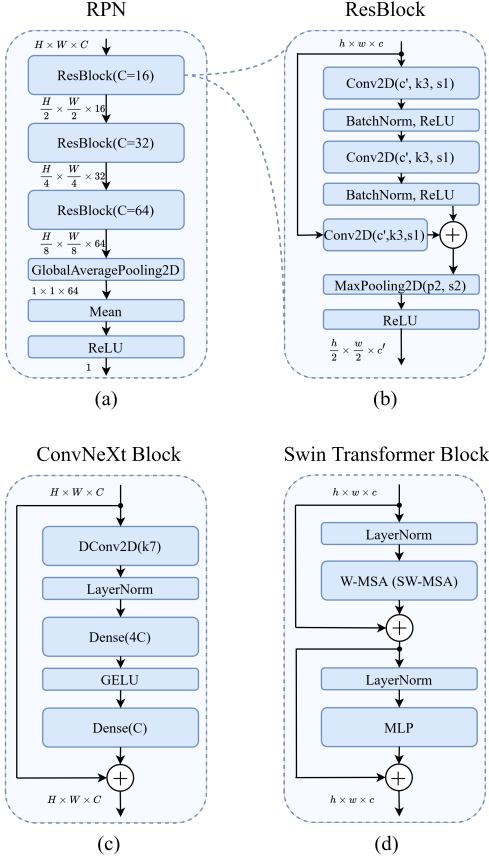


Fig. 3. Detailed description of block architectures: (a) RPN, (b) ResBlock, (c) ConvNeXt Block, and (d) Swin Transformer Block. DConv2D(.) stands for depthwise 2D convolution, LayerNorm for the layer normalization, Dense(.) for the densely-connected neural network layer, and GELU for the activation.

tized latents \hat{y} and \hat{z} feed the synthesis and hyper-synthesis transforms, respectively, to generate the reconstructed image. The decoder schemes are symmetric to those of the encoder, with patch-merging layers replaced by patch-expanding layers.

The Swin Transformer block architecture, depicted in Fig. 3 (d), is a variant of the vision transformer (ViT) that has recently gained attention due to its superior performance on a range of computer vision tasks. Therefore, it is essential to highlight the unique features and advantages to motivate the choice of the Swin Transformer over other ViT variants. One key advantage of the Swin Transformer is its hierarchical design, which enables it to process images of various resolutions efficiently. Unlike other ViT variants, Swin Transformer divides the image into smaller patches at multiple scales, allowing it to capture both local and global information. This hierarchical design has been shown to be particularly effective for large-scale vision tasks. Another advantage of the Swin Transformer is its ability to incorporate spatial information into its attention mechanism. Swin Transformer introduces a novel shifted window attention mechanism, which aggregates information from neighboring patches in a structured way, allowing it to capture spatial relationships between image features, leading to linear complexity w.r.t. the input resolution. This attention mechanism has been shown to outperform the standard ViT attention mechanism, whose complexity is quadratic, on a range of benchmarks. Overall,

Swin Transformer’s efficiency and superior performance make it a promising architecture for NIC. In addition, its ability to capture both global and local features efficiently, and its adaptability to different image resolutions, make it a strong contender among other transformer-based architectures.

E. Transformer-based Slice Transform

In the realm of neural image compression, incorporating spatio-channel dependencies into entropy modeling is crucial. These dependencies, often termed spatial and channel or spatial-channel dependencies in prior literature [21], [52], capture the intricate relationships among neighboring pixels within quantized latent features across different channels. Recognizing these spatio-channel dependencies in the quantized latent representation is essential for eliminating redundancy along spatial and channel axes, ultimately enhancing compression efficiency while maintaining perceptual quality. Aligned with this objective, we introduce the concept of separate entropy coding by partitioning the hyperprior latent representation into channel groups, as opposed to the conventional serial-decoded approach, to achieve more effective context modeling. Subsequently, we propose a tiny Transformer-based spatial context model that leverages cross-channel redundancies to generate highly informative adjacent contexts from the hyperprior latent slices, combined with the already-decoded latent slices. Consequently, our approach introduces a multidimensional entropy estimation model known as spatio-channel entropy modeling, which proves to be both fast and effective in reducing bitrate. According to this method, each latent element is conditioned on adjacent decoded elements that are spatio-channel neighbors, effectively eliminating redundancy along spatial and channel axes.

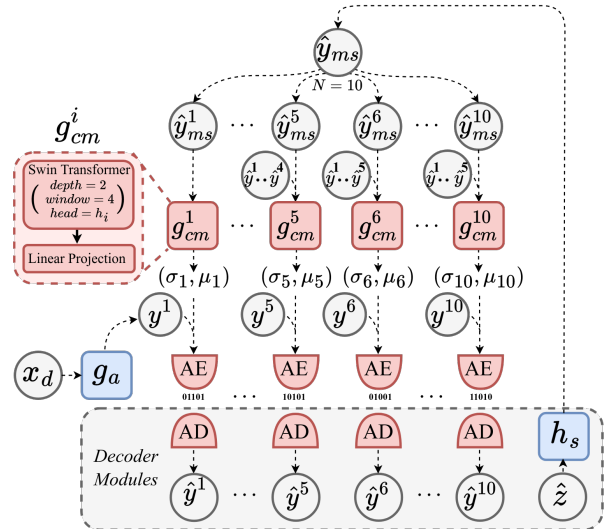


Fig. 4. Spatio-channel entropy coding. g_a , h_s , g_{cm}^i , AE, and AD stand for analysis and hyper-synthesis transforms, the i^{th} context model, and arithmetic encoder/decoder, respectively. $\{y^1, \dots, y^s\}$ stands for the already-decoded latent slices, where $\{s \in \mathbb{N} \mid 1 \leq s \leq 5\}$ is the number of supported slices.

Fig. 4 shows our spatio-channel entropy coding. We apply a tiny spatial context model g_{cm}^i to exploit the spatio-channel correlations per i^{th} grouped hyperprior channels \hat{y}_{ms}^i

TABLE I
ARCHITECTURE CONFIGURATION.

IC	Filter size C_i						Depth size d_i							
	C_1	C_2	C_3	C_4	C_5	C_6	d_0	d_1	d_2	d_3	d_4	d_5	d_6	d_7
B1	320	320	320	320	192	192	—	—	—	—	—	—	—	—
B2	128	192	256	320	192	192	—	2	2	6	2	5	1	—
O1	128	192	256	320	192	192	—	2	2	6	2	5	1	2
O2	128	192	256	320	192	192	3	2	2	6	2	5	1	2

combined with the already-decoded latent slices $\{y^1, \dots, y^s\}$, where $\{s \in \mathbb{N} \mid 1 \leq s \leq 5\}$ stands for the number of supported slices. This process enhances the accuracy of entropy parameter estimation, thereby optimizing the overall efficiency of entropy coding.

As a side effect, it also results in faster decoding speed, thanks to the parallelization capabilities of the Swin Transformer on graphics processing unit (GPU) [29]. In contrast to ConvNets that rely on convolution in place of general matrix multiplication and are susceptible to communication overhead when parallelizing across multiple GPUs, Swin Transformers exhibit better parallelizability on GPUs. This is attributed to their hierarchical attention mechanism, which processes attention in a windowed manner, reducing global attention complexity and enabling efficient self-attention parallelization. Additionally, Swin Transformers leverage multi-head parallelism and tokenization strategies to maximize GPU utilization. These features make them a prime choice for a wide range of computer vision tasks that require GPU acceleration. The tiny slice transform consists of two successive Swin Transformer blocks with an additional learnable linear projection layer, used to get a representative latent slices concatenation. This ChARM estimates the distribution $p_{\hat{y}}(\hat{y}|\hat{z})$ with both the mean and standard deviation of each quantized latent slice and incorporates an autoregressive context model to condition the already-decoded latent slices and further reduce the spatial redundancy between adjacent pixels.

IV. EXPERIMENTAL RESULTS

In this section, we first describe the experimental setup, including the used datasets, the baselines against which we compared, and the implementation details. Then, we assess the compression efficiency of our method with a rate-distortion comparison and compute the average bitrate savings on four commonly-used evaluation datasets. We further elaborate a model scaling study to consistently examine the effectiveness of our proposed method against pioneering ones. Additionally, we perform a resize parameter analysis to show the variations of the predicted parameter s . Finally, we conduct a latent analysis, an ablation study, and a qualitative analysis to highlight the impact of our architectural choices.

A. Experimental Setup

Datasets. The training set of the CLIC2020 dataset is used to train the proposed models. This dataset contains professional and user-generated content images in RGB color and grayscale formats. We evaluate image compression models on four datasets, including Kodak [53], Tecnick [54],

JPEG-AI [55], and the testing set of CLIC21 [56]. Fig. 5 gives the number of images by pixel count for the four test datasets. Finally, for a fair comparison, all images are cropped to the highest possible multiples of 256 to avoid padding for neural codecs.

Baselines. We compare our approach with the state-of-art neural compression method SwinT-ChARM proposed by Zhu *et al.* [16], and the Conv-ChARM proposed by Minnen *et al.* [15], and non-neural compression methods, including better portable graphics (BPG)(4:4:4), and the up-to-date VVC official Test Model VTM-18.0 in All-Intra profile configuration. Table I gives the configuration of each of the considered image codec baselines with B1 and B2 referring to Conv-ChARM and SwinT-ChARM, respectively, and O1 and O2 refer to our proposed approaches ICT and AICT, respectively. C_i and d_i are the hyperparameters defined in Fig. 2. We intensively compare our solutions with Conv-ChARM [15] and SwinT-ChARM [16] from the state-of-the-art models [17], [18], [20]–[22], [25], under the same training and testing conditions. Nevertheless, Fig. 9 compares our models with additional state-of-the-art solutions.

Implementation details. We implemented all models in TensorFlow using tensorflow compression (TFC) library [57], and the experimental study was carried out on an RTX 5000 Ti GPU. All models were trained on the same CLIC2020 training set with 2M steps using the ADAM optimizer with parameters $\beta_1 = 0.9$ and $\beta_2 = 0.999$. The initial learning rate is set to 10^{-4} and drops to 10^{-5} for the last 200k iterations. The loss function, expression in Equation (7), is a weighted combination of bitrate R and distortion D , with λ being the Lagrangian multiplier steering rate-distortion trade-off. MSE is used as the distortion metric in RGB color space. Each training batch contains eight random crops $x^j \in R^{256 \times 256 \times 3}$ from the CLIC2020 training set. To cover a wide range of rate and distortion points, for our proposed method and respective ablation models, we trained four models with $\lambda \in \{1000, 200, 20, 3\} \times 10^{-5}$. The inference time experiments on the central processing unit (CPU) are performed on an Intel(R) Xeon(R) W-2145 processor running at 3.70 GHz.

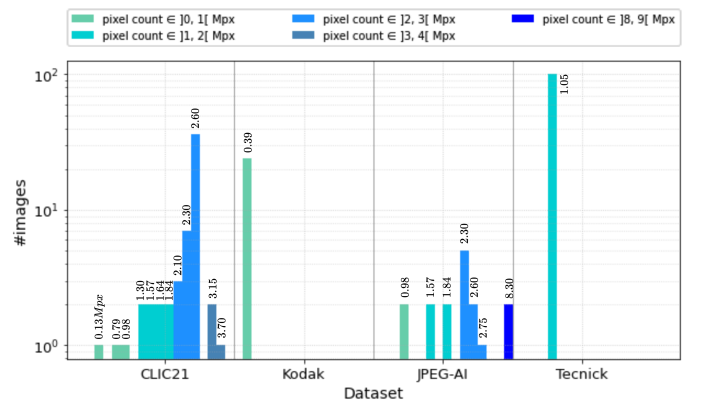


Fig. 5. Number of images per dataset per pixel count in megapixel (Mpx).

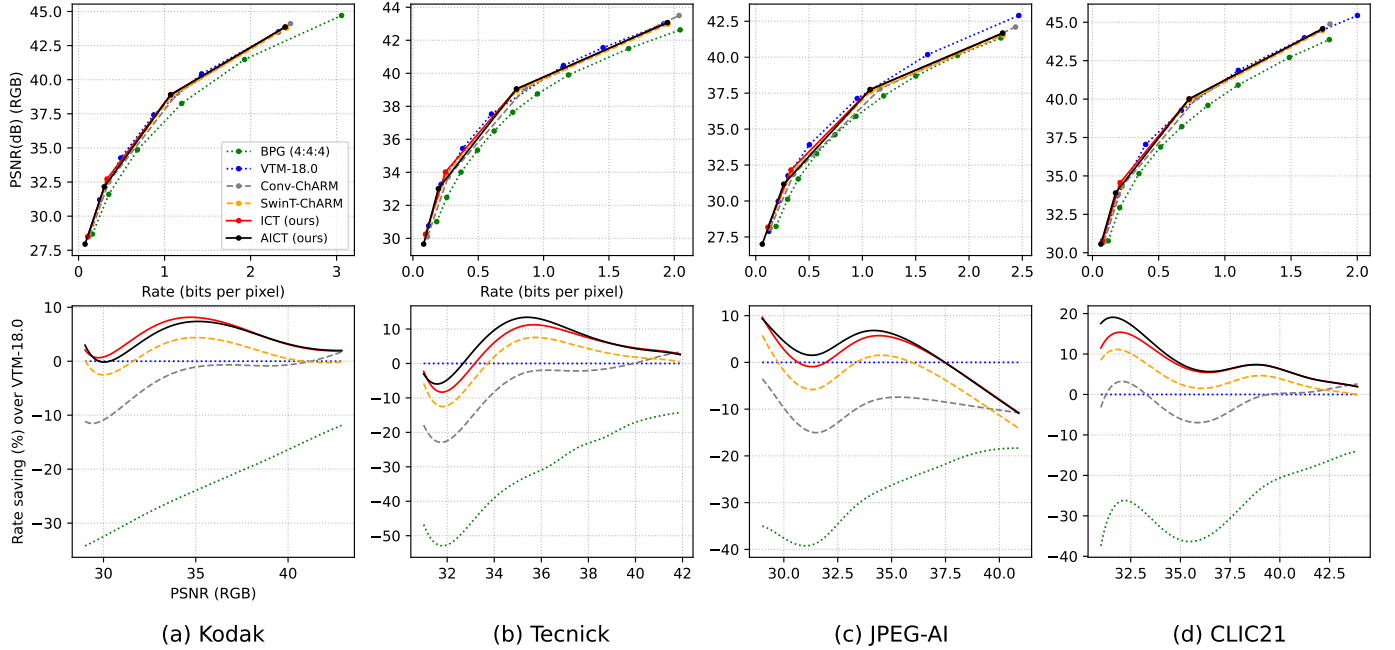


Fig. 6. Comparison of compression efficiency on Kodak, Tecnick, JPEG-AI, and CLIC21 datasets. Rate-distortion (PSNR vs. rate (bpp)) comparison and rate saving over VTM-18.0 (larger is better) are respectively illustrated for each benchmark dataset.

TABLE II

BD-RATE \downarrow (PSNR) PERFORMANCE OF BPG (4:4:4), CONV-CHARM, SWIN-T-CHARM, ICT, AND AICT COMPARED TO THE VTM-18.0.

Image Codec	Kodak	Tecnick	JPEG-AI	CLIC21	Average
BPG444	22.28%	28.02%	28.37%	28.02%	26.67%
Conv-ChARM	2.58%	3.72%	9.66%	2.14%	4.53%
SwinT-ChARM	-1.92%	-2.50%	2.91%	-3.22%	-1.18%
ICT (ours)	-5.10%	-5.91%	-1.14%	-6.44%	-4.65%
AICT (ours)	-5.09%	-5.99%	-2.03%	-7.33%	-5.11%

B. Rate-Distortion Performance

To demonstrate the compression efficiency of our proposed solutions, we plot the rate-distortion curves of ICT, AICT, and the baselines on benchmark datasets. Fig. 6 (a) (1st row) gives the PSNR versus the bitrate for our solutions and baselines on the Kodak dataset. The latter figure shows that AICT and ICT equally outperform the neural approaches Conv-ChARM and SwinT-ChARM, as well as BPG(4:4:4) and VTM-18.0 traditional codecs, achieving a higher PSNR values for the different bitrate ranges.

Moreover, we introduce Fig. 6 (a) (2nd row), showing the rate savings over the VTM-18.0 on the Kodak dataset. The rate saving over VVC (%) represents the percentage reduction in bitrate achieved by a specific compression model compared to a reference codec while maintaining an equivalent level of image reconstruction quality, as measured by peak signal-to-noise ratio (PSNR) in our context. This graph is a generalized version of a Bjøntegaard Delta (BD) chart [58] by plotting rate savings as a function of quality, instead of solely presenting average savings [15]. By comparing the performance of different models using this figure, we can discern which model excels in striking a balance between compression efficiency at

TABLE III

BD-RATE \downarrow PERFORMANCE OF SWIN-T-CHARM, ICT, AND AICT COMPARED TO THE CONV-CHARM.

Image Codec	Kodak	Tecnick	JPEG-AI	CLIC21	Average
BD-rate (PSNR) \downarrow					
SwinT-ChARM	-4.24%	-6.40%	-6.13%	-5.37%	-5.54%
ICT (ours)	-7.30%	-9.52%	-9.85%	-8.47%	-8.79%
AICT (ours)	-7.28%	-9.68%	-10.20%	-9.35%	-9.13%
BD-rate (MS-SSIM) \downarrow					
SwinT-ChARM	-6.34%	-7.01%	-7.49%	-6.30%	-6.79%
ICT (ours)	-7.60%	-8.31%	-9.29%	-7.50%	-8.18%
AICT (ours)	-7.58%	-8.31%	-9.87%	-7.67%	-8.36%

different levels of reconstruction quality. Models that achieve higher bitrate savings over VVC at various PSNR levels are considered superior in terms of compression performance. ICT and AICT achieve significant rate savings compared to the baselines, demonstrating their ability to compress images more efficiently. More specifically, AICT, including the adaptive resolution module, achieves the highest bitrate gain at a low bitrate/quality range, where it is more beneficial to reduce the spatial resolution. To further generalize the effectiveness of our solutions, we extend the evaluation to three high resolutions datasets (Tecnick, JPEG-AI, and CLIC21), as shown in Fig. 6. The figure illustrates the PSNR versus bitrate (1st row), rate savings (2nd row) on the considered datasets. AICT and ICT consistently achieve better rate-distortion performance and considerable rate savings compared to the existing traditional codecs and the neural codecs Conv-ChARM and SwinT-ChARM, demonstrating their efficiency across different high-resolution images and datasets.

Furthermore, we assessed the effectiveness of our meth-

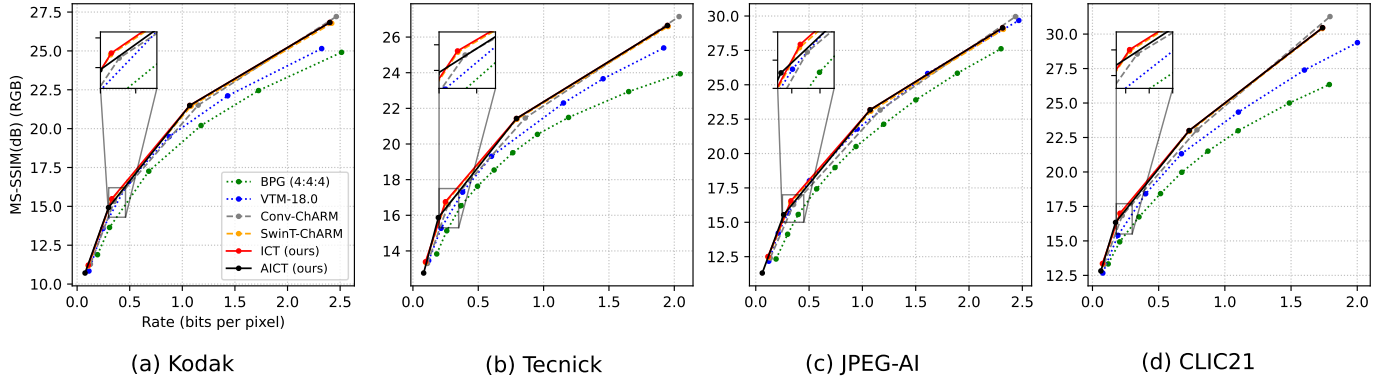


Fig. 7. Comparison of compression efficiency on the Kodak, Tecnick, JPEG-AI, and CLIC21 datasets. Rate distortion (MS-SSIM vs the rate (bpp)) comparison is illustrated for each benchmark dataset.

ods using the perceptual quality metric multi-scale structural similarity index (MS-SSIM) on the four benchmark datasets. To calculate MS-SSIM in decibels (dB), a logarithmic transformation is applied to the original MS-SSIM values as follows: $MSSSIM(dB) = -10 \times \log_{10}(1 - MSSSIM)$. This transformation is performed to provide a more intuitive and interpretable scale for comparing image quality, as previously done in several works [18], [20]–[22], [59]. Fig. 7 gives the MS-SSIM scores expressed versus the bitrate for the four test datasets. As illustrated in Fig. 7, our methods yield better coding performance than the current neural baselines in terms of MS-SSIM. Note that we haven’t optimized our approaches and baselines using MS-SSIM, as a differentiable distortion measure in the loss function, during the training process. Thus, optimizing the solutions with MS-SSIM will further improve the performance regarding this metric.

Besides the rate-distortion rate savings curves, we also evaluate different models using Bjontegaard’s metric [58], which computes the average bitrate savings (%) between two rate-distortion curves. In Table II, we summarize the BD-rate (PSNR) of image codecs across all four datasets, compared to the VTM-18.0 as the anchor. On average, ICT and AICT are able to respectively achieve -4.65% and -5.11% rate reductions compared to VTM-18.0 and -3.47% and -3.93% relative gain from SwinT-ChARM. In addition, Table III presents the BD-rate (PSNR/MS-SSIM) of SwinT-ChARM, ICT, and AICT across the considered datasets, compared with the anchor Conv-ChARM. Once again, ICT and AICT are able to outperform the neural approach Conv-ChARM, with average rate reductions (PSNR) of -8.79% and -9.13% and average rate reductions (MS-SSIM) of -8.18% and -8.36%, respectively, outperforming SwinT-Charm solution on the four benchmark datasets and the two image quality metrics.

Overall, the proposed ICT and AICT have demonstrated strong rate-distortion performance on various benchmark datasets. This indicates that our approaches can better preserve image quality at lower bitrates, highlighting its potential for practical applications in image compression.

C. Models Scaling Study

We evaluated the decoding complexity of the proposed and baseline neural codecs by averaging decoding time across 7000

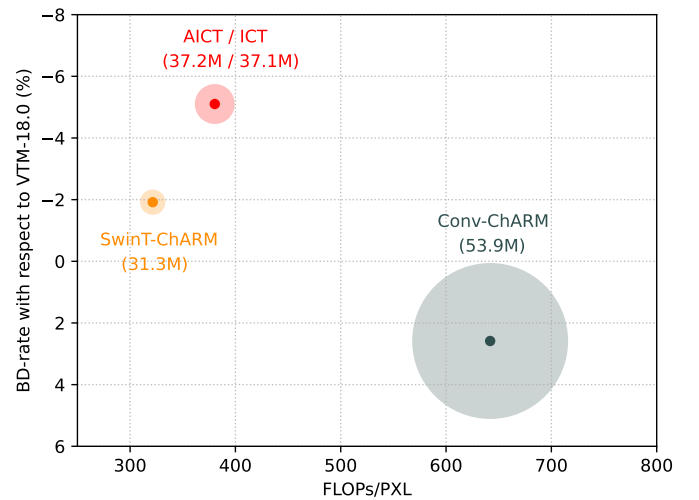


Fig. 8. Model size scaling. BD-rate (PSNR) on Kodak dataset versus FLOPs per pixel for the proposed AICT and ICT compared to Conv-ChARM and SwinT-ChARM (for both encoding and decoding). Circle sizes indicate the numbers of parameters. Left-top is better.

images at $256 \times 256 \times 3$ resolution, encoded at varying bitrates, specifically $\{0.1, 0.8, 1.5\}$ (bpp). Subsequently, we computed the average decoding time for this dataset, resulting in an overall average bit rate of 0.8bpp. Table IV gives the image codec complexity features, including the decoding time on GPU and CPU, floating point operations per second (FLOPs), and the total model parameters. Finally, we recall that the models run with Tensorflow 2.8 on a workstation with one RTX 5000 Ti GPU.

Compared to the neural baselines, ICT can achieve faster decoding speed on GPU but not on CPU, which proves the parallel processing ability to speed up compression on GPU and the well-engineered designs of both transform and entropy coding. This is potentially helpful for conducting high-quality real-time visual data streaming. Our AICT is on par with ICT in terms of the number of parameters, FLOPs, and latency, indicating the lightweight nature of the scale adaptation module with consistent coding gains over four datasets and two quality metrics.

Fig. 8 gives the BD-rate (with VTM-18.0 as an anchor)

TABLE IV
IMAGE CODEC COMPLEXITY. WE CALCULATED THE AVERAGE DECODING LATENCY ACROSS 7000 IMAGES AT 256×256 RESOLUTION, ENCODED ON AVERAGE AT 0.8 BPP. THE BEST SCORE IS HIGHLIGHTED IN BOLD.

Image Codec	Latency(ms)↓		MFLOPs↓	#parameters (M)↓
	GPU	CPU		
Conv-ChARM	133.8	359.8	126.1999	53.8769
SwinT-ChARM	91.8	430.7	63.2143	31.3299
ICT (ours)	80.1	477.0	74.7941	37.1324
AICT (ours)	88.3	493.3	74.9485	37.2304

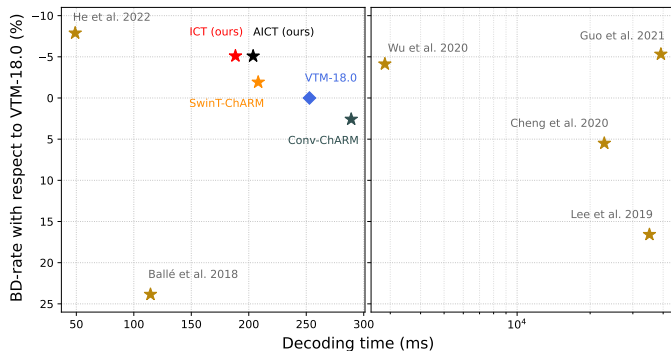


Fig. 9. BD-rate (PSNR) versus decoding time (ms) on the Kodak dataset. Star and diamond markers refer to decoding on GPU and CPU, respectively. Left-top is better.

performance versus the FLOPs per pixel of the ICT, AICT, SwinT-ChARM and Conv-ChARM on the Kodak dataset. We can notice that ICT and AICT are in an interesting area, achieving a good trade-off between BD-rate score on Kodak, total model parameters, and FLOPs per pixel, reflecting an efficient and hardware-friendly compression model.

Finally, Fig. 9 shows the BD-rate (with VTM-18.0 as an anchor) versus the decoding time of various codecs on the Kodak dataset. It can be seen from the figure that our ICT and AICT achieve a good trade-off between BD-rate performance and decoding time. Furthermore, the symmetrical architecture of the proposed solutions allows similar complexity at both the encoder and decoder. This feature can be an advantage of neural codecs, since the best conventional codecs like VVC exhibit more complex encoding than decoding.

D. Resize Parameter Analysis

We conduct a resize parameter analysis through the benchmark datasets, including the images of the four datasets with various resolutions, as illustrated in Fig. 5.

Fig. 10 shows how the parameter s varies according to the weighting parameter λ (i.e., bitrate) for the four datasets. First, we can notice that the estimated resize parameter s depends on the bitrate and the spatial characteristics of the image content. Resizing the input image to a lower resolution is frequently observed at a low bitrate, where the compression removes the image details. In contrast, the down-sampling is not performed at a high bitrate to reach high image quality, significantly when the up-sampling module cannot recover the image details at the decoder. Nevertheless, even at a high bitrate, a few samples are down-sampled to a lower resolution,

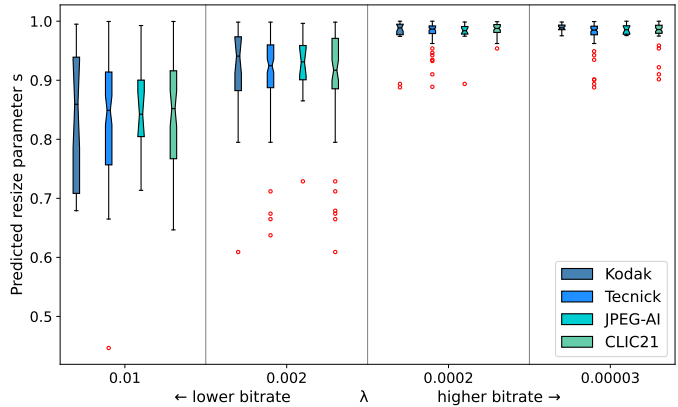


Fig. 10. Box plot of predicted resize parameter s versus the weighting parameter λ , evaluated across the four considered datasets. The 'o' symbol denotes outliers.

especially images with low spatial information that the up-sampling module can easily recover on the decoder side. This also can explain the higher coding gain brought by the adaptive sampling module of AICT on datasets, including more high-resolution images such as JPEG-AI and CLIC21 (see Fig. 5). To gain a deeper understanding of the observed performance variations in Tables II and III, we direct our focus towards the characteristics of the test datasets. Illustrated in Fig. 5, the distribution of images by pixel count for the four test datasets, including Kodak, Tecnick, and two datasets (JPEG-AI and CLIC21) with higher-resolution images. It is noteworthy that, as depicted in the Fig. 5, Kodak and Tecnick comprise images with a significantly lower total number of pixels. This particular attribute inherently impacts the effectiveness of certain modules, like adaptive scaling, given the correlation between the predicted resize factor and the total number of pixels in each image. Furthermore, the content complexity within these datasets may contribute to the observed limited impact of adaptive scaling. As demonstrated in the Fig. 10, images with higher high-frequency details might not experience as significant benefits from such modules. In addition, skipping the resize modules for a predicted scale close to $s \cong 1$ contribute to reducing encoding and decoding complexity.

E. Latent Analysis

Transform coding is motivated by the idea that coding is more effective in the transform domain than in the original signal space. A desirable transform would decorrelate the source signal so that a simple scalar quantization and factorized entropy model can be applied without constraining coding performance. Furthermore, an appropriate prior model would provide context adaptivity and utilize distant spatial relations in the latent tensor. The effectiveness of the analysis transforms g_a can then be evaluated by measuring the level of correlation in the latent signal \hat{y} . We are particularly interested in measuring the correlation between nearby spatial positions, which are heavily correlated in the source domain for natural images. In Fig. 11, we visualize the normalized spatial correlation of \hat{y} averaged over all latent channels and compare Conv-ChARM and SwinT-ChARM with the proposed ICT at $\lambda = 0.002$. We

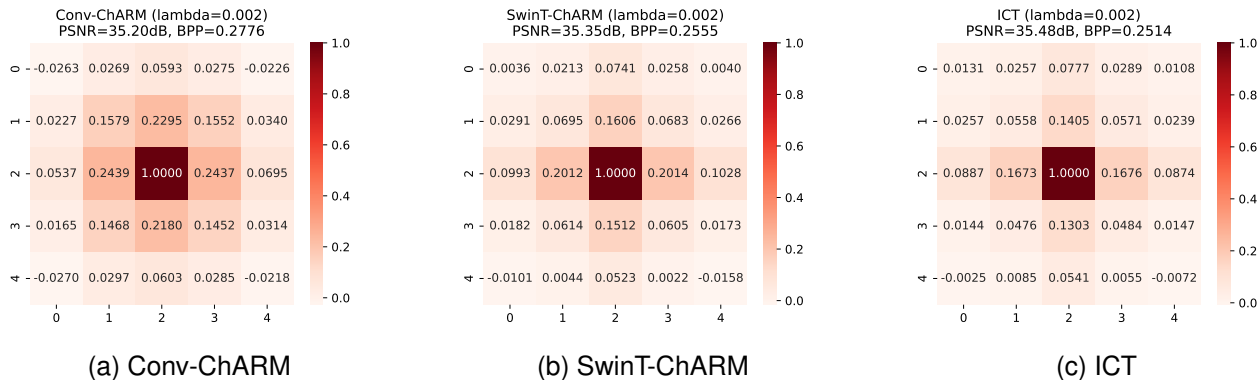


Fig. 11. The spatial correlation at index (i, j) corresponds to the normalized cross-correlation of the reconstructed latent $\frac{(\hat{y}_i - \mu)}{\sigma}$ at spatial location (w_c, h_c) and $(w_c + i, h_c + j)$, averaged across all latent channels of all image patches across the four considered datasets. We considered (a) Conv-ChARM, (b) SwinT-ChARM, and the proposed (c) ICT, all trained at $\lambda = 0.002$.

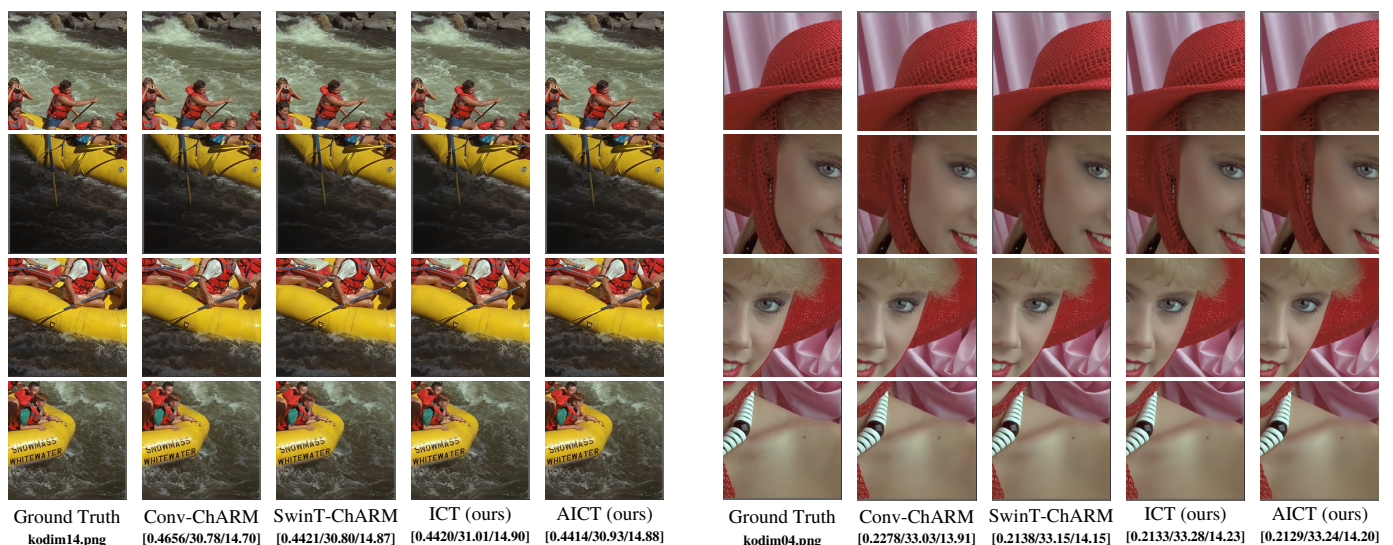


Fig. 12. Visualization of the reconstructed images from the Kodak dataset. The metrics are $[\text{bpp} \downarrow / \text{PSNR}(\text{dB}) \uparrow / \text{MS-SSIM}(\text{dB}) \uparrow]$.

can observe that while both lead to small cross-correlations, ICT can decorrelate the latent with a slight improvement when compared to SwinT-ChARM and a much considerable improvement when compared to Conv-ChARM. This suggests that Transformer-based transforms with Transformer-based entropy modeling incur less redundancy across different spatial latent locations than convolutional ones, leading to an overall better rate-distortion trade-off.

F. Ablation Study

To investigate the impact of the proposed ICT and AICT, we conduct an ablation study according to the reported BD-rate \downarrow w.r.t. VVC and Conv-ChARM in Table II and Table III, respectively. Image compression performance increases from Conv-ChARM to SwinT-ChARM on the considered datasets due to the inter-layer feature propagation across non-overlapping windows (local information) and self-attention mechanism (long-range dependencies) in the Swin Transformer. With the proposed spatio-channel entropy model, ICT is able to achieve on average -3.47% (PSNR) and -1.39% (MS-SSIM)

rate reductions compared to SwinT-ChARM. Moreover, AICT is enhancing ICT on average by -0.46% (PSNR) and -0.18% (MS-SSIM) rate reductions with consistent gain over the four datasets. This indicates that introducing a scale adaptation module can further reduce spatial redundancies and alleviate coding artifacts, especially at low bitrate for higher compression efficiency. More importantly, the adaptive resolution may also reduce the complexity of the encoder and decoder regarding the number of operations per pixel since fewer pixels are processed on average by the codec when the input image is downscaled to a lower resolution, i.e., $s < 1$.

G. Qualitative Analysis

To assess the perceptual quality of the decoded images, we visualize two reconstructed samples with the proposed ICT and AICT methods, along with Conv-ChARM and SwinT-ChARM, all trained at the same low bitrate configuration ($\lambda = 0.002$). Fig. 12 presents the visualization of the reconstructed *kodim14* and *kodim04* images from the Kodak dataset. Although not immediately apparent in Fig. 12, the proposed

ICT and AICT may manifest subtle improvements in specific image regions or content types. A closer examination reveals discernible differences in certain areas of the reconstructed images. For instance, in the 'kodim14.png' figure, there is a noticeable enhancement in the intensity of black pixels within the text elements in the proposed models, ICT and AICT, compared to the baselines. This signifies a finer level of detail preservation in the text, which can be particularly crucial in applications involving textual content. Moreover, in the same 'kodim14.png' figure, in the last row of patches, it can be observed that the representation of water soaking the green sweater worn by the person is significantly better in the ICT model compared to the other models. This improved depiction of intricate textures and finer details highlights the model's capability to faithfully capture and reproduce complex image features, which may be essential in scenarios where preserving fine textures is critical for maintaining perceptual quality. In summary, under a similar rate budget, ICT and AICT perform better in maintaining texture details and clean edges while suppressing visual artifacts of the decoded images compared to Conv-ChARM and SwinT-ChARM neural approaches. Additionally, the self-attention mechanism focuses more on high-contrast image regions and consequently achieves more coding efficiency on such content.

V. CONCLUSION

In this work, we have proposed an up-and-coming neural codec AICT, achieving compelling rate-distortion performance while significantly reducing the latency, which is potentially helpful to conduct, with further optimizations, high-quality real-time visual data transmission. We inherited the advantages of self-attention units from Transformers to approximate the mean and standard deviation for efficient entropy modeling and combine global and local texture to capture correlations among spatially neighboring elements for non-linear transform coding. Furthermore, we have presented a lightweight spatial resolution scale adaptation module to enhance compression ability, especially at low bitrates. The experimental results, conducted on four datasets, showed that ICT and AICT approaches outperform the state-of-the-art conventional codec VVC, achieving respectively -4.65% and -5.11% BD-rate reductions compared to the VTM-18.0 by averaging over the benchmark datasets. With the development of GPU and neural processing unit (NPU) chip technologies and further engineering optimization, neural codecs will be the future of visual data coding, achieving better compression efficiency when compared with traditional codecs and aiming to bridge the gap to a real-time processing.

VI. ACKNOWLEDGEMENTS

This work has been supported by Région Bretagne and Rennes Ville et Métropole under the DEEPTEC project.

REFERENCES

[1] G. Wallace, "The jpeg still picture compression standard," *IEEE Transactions on Consumer Electronics*, vol. 38, no. 1, pp. xviii–xxxiv, 1992.

[2] M. Gormish, D. Lee, and M. Marcellin, "Jpeg 2000: overview, architecture, and applications," in *Proceedings 2000 International Conference on Image Processing (Cat. No.00CH37101)*, vol. 2, 2000, pp. 29–32 vol.2.

[3] G. J. Sullivan, J.-R. Ohm, W.-J. Han, and T. Wiegand, "Overview of the high efficiency video coding (hevc) standard," *IEEE Transactions on Circuits and Systems for Video Technology*, vol. 22, no. 12, pp. 1649–1668, 2012.

[4] B. Bross, Y.-K. Wang, Y. Ye, S. Liu, J. Chen, G. J. Sullivan, and J.-R. Ohm, "Overview of the versatile video coding (vvc) standard and its applications," *IEEE Transactions on Circuits and Systems for Video Technology*, vol. 31, no. 10, pp. 3736–3764, 2021.

[5] S. Ma, X. Zhang, C. Jia, Z. Zhao, S. Wang, and S. Wang, "Image and video compression with neural networks: A review," *IEEE Transactions on Circuits and Systems for Video Technology*, vol. 30, no. 6, pp. 1683–1698, 2020.

[6] J. Ballé, D. Minnen, S. Singh, S. J. Hwang, and N. Johnston, "Variational image compression with a scale hyperprior," in *International Conference on Learning Representations*, 2018.

[7] Y. Hu, W. Yang, and J. Liu, "Coarse-to-fine hyper-prior modeling for learned image compression," in *Proceedings of the AAAI Conference on Artificial Intelligence*, vol. 34, 2020, pp. 11 013–11 020.

[8] D. Minnen, J. Ballé, and G. D. Toderici, "Joint autoregressive and hierarchical priors for learned image compression," *Advances in neural information processing systems*, vol. 31, 2018.

[9] J. Lee, S. Cho, S. Yoon Jeong, H. Kwon, H. Ko, H. Yong Kim, and J. Soo Choi, "Extended end-to-end optimized image compression method based on a context-adaptive entropy model," in *Proceedings of the IEEE/CVF Conference on Computer Vision and Pattern Recognition (CVPR) Workshops*, June 2019.

[10] Z. Cheng, H. Sun, M. Takeuchi, and J. Katto, "Learned image compression with discretized gaussian mixture likelihoods and attention modules," in *Proceedings of the IEEE/CVF Conference on Computer Vision and Pattern Recognition*, 2020, pp. 7939–7948.

[11] M. Li, K. Zhang, J. Li, W. Zuo, R. Timofte, and D. Zhang, "Learning context-based nonlocal entropy modeling for image compression," *IEEE Transactions on Neural Networks and Learning Systems*, vol. 34, no. 3, pp. 1132–1145, 2023.

[12] Y. Qian, Z. Tan, X. Sun, M. Lin, D. Li, Z. Sun, L. Hao, and R. Jin, "Learning accurate entropy model with global reference for image compression," in *International Conference on Learning Representations*, 2021.

[13] T. Chen, H. Liu, Z. Ma, Q. Shen, X. Cao, and Y. Wang, "End-to-end learnt image compression via non-local attention optimization and improved context modeling," *IEEE Transactions on Image Processing*, vol. 30, pp. 3179–3191, 2021.

[14] F. Mentzer, G. D. Toderici, M. Tschannen, and E. Agustsson, "High-fidelity generative image compression," *Advances in Neural Information Processing Systems*, vol. 33, pp. 11 913–11 924, 2020.

[15] D. Minnen and S. Singh, "Channel-wise autoregressive entropy models for learned image compression," in *2020 IEEE International Conference on Image Processing (ICIP)*. IEEE, 2020, pp. 3339–3343.

[16] Y. Zhu, Y. Yang, and T. Cohen, "Transformer-based transform coding," in *International Conference on Learning Representations*, 2021.

[17] R. Zou, C. Song, and Z. Zhang, "The devil is in the details: Window-based attention for image compression," in *Proceedings of the IEEE/CVF Conference on Computer Vision and Pattern Recognition*, 2022, pp. 17 492–17 501.

[18] X. Zhu, J. Song, L. Gao, F. Zheng, and H. T. Shen, "Unified multivariate gaussian mixture for efficient neural image compression," in *Proceedings of the IEEE/CVF Conference on Computer Vision and Pattern Recognition*, 2022, pp. 17 612–17 621.

[19] Z. Guo, Z. Zhang, R. Feng, and Z. Chen, "Causal contextual prediction for learned image compression," *IEEE Transactions on Circuits and Systems for Video Technology*, vol. 32, no. 4, pp. 2329–2341, 2022.

[20] J.-H. Kim, B. Heo, and J.-S. Lee, "Joint global and local hierarchical priors for learned image compression," in *Proceedings of the IEEE/CVF Conference on Computer Vision and Pattern Recognition*, 2022, pp. 5992–6001.

[21] D. He, Z. Yang, W. Peng, R. Ma, H. Qin, and Y. Wang, "Elic: Efficient learned image compression with unevenly grouped space-channel contextual adaptive coding," in *Proceedings of the IEEE/CVF Conference on Computer Vision and Pattern Recognition*, 2022, pp. 5718–5727.

[22] A. El-Nouby, M. J. Muckley, K. Ullrich, I. Laptev, J. Verbeek, and H. Jegou, "Image compression with product quantized masked image modeling," *Transactions on Machine Learning Research*, 2023.

- [23] H. Jegou, C. Schmid, H. Harzallah, and J. Verbeek, "Accurate image search using the contextual dissimilarity measure," *IEEE Transactions on Pattern Analysis and Machine Intelligence*, vol. 32, no. 1, pp. 2–11, 2008.
- [24] A. Van den Oord, N. Kalchbrenner, L. Espeholt, O. Vinyals, A. Graves *et al.*, "Conditional image generation with pixelcnn decoders," *Advances in neural information processing systems*, vol. 29, 2016.
- [25] M. J. Muckley, A. El-Nouby, K. Ullrich, H. Jégou, and J. Verbeek, "Improving statistical fidelity for neural image compression with implicit local likelihood models," *arXiv preprint arXiv:2301.11189*, 2023.
- [26] E. Dupont, A. Golinski, M. Alizadeh, Y. W. Teh, and A. Doucet, "COIN: COmpression with implicit neural representations," in *Neural Compression: From Information Theory to Applications – Workshop @ ICLR 2021*, 2021.
- [27] Y. Strümpfer, J. Postels, R. Yang, L. V. Gool, and F. Tombari, "Implicit neural representations for image compression," in *Computer Vision–ECCV 2022: 17th European Conference, Tel Aviv, Israel, October 23–27, 2022, Proceedings, Part XXVI*. Springer, 2022, pp. 74–91.
- [28] Y. Wu, X. Li, Z. Zhang, X. Jin, and Z. Chen, "Learned block-based hybrid image compression," *IEEE Transactions on Circuits and Systems for Video Technology*, vol. 32, no. 6, pp. 3978–3990, 2022.
- [29] Z. Liu, Y. Lin, Y. Cao, H. Hu, Y. Wei, Z. Zhang, S. Lin, and B. Guo, "Swin transformer: Hierarchical vision transformer using shifted windows," in *Proceedings of the IEEE/CVF International Conference on Computer Vision*, 2021, pp. 10012–10022.
- [30] Z. Liu, H. Mao, C.-Y. Wu, C. Feichtenhofer, T. Darrell, and S. Xie, "A convnet for the 2020s," in *Proceedings of the IEEE/CVF Conference on Computer Vision and Pattern Recognition*, 2022, pp. 11976–11986.
- [31] Y. Choi, M. El-Khamy, and J. Lee, "Variable rate deep image compression with a conditional autoencoder," in *Proceedings of the IEEE/CVF International Conference on Computer Vision*, 2019, pp. 3146–3154.
- [32] M. Li, W. Zuo, S. Gu, J. You, and D. Zhang, "Learning content-weighted deep image compression," *IEEE transactions on pattern analysis and machine intelligence*, vol. 43, no. 10, pp. 3446–3461, 2020.
- [33] H. Ma, D. Liu, N. Yan, H. Li, and F. Wu, "End-to-end optimized versatile image compression with wavelet-like transform," *IEEE Transactions on Pattern Analysis and Machine Intelligence*, vol. 44, no. 3, pp. 1247–1263, 2022.
- [34] K. Gregor, F. Besse, D. Jimenez Rezende, I. Danihelka, and D. Wierstra, "Towards conceptual compression," *Advances In Neural Information Processing Systems*, vol. 29, 2016.
- [35] B. J. Frey, *Bayesian networks for pattern classification, data compression, and channel coding*. Citeseer, 1997.
- [36] A. Alemi, B. Poole, I. Fischer, J. Dillon, R. A. Saurous, and K. Murphy, "Fixing a broken elbo," in *International conference on machine learning*. PMLR, 2018, pp. 159–168.
- [37] D. He, Y. Zheng, B. Sun, Y. Wang, and H. Qin, "Checkerboard context model for efficient learned image compression," in *Proceedings of the IEEE/CVF Conference on Computer Vision and Pattern Recognition*, 2021, pp. 14771–14780.
- [38] M.-T. Luong, H. Pham, and C. D. Manning, "Effective approaches to attention-based neural machine translation," *arXiv preprint arXiv:1508.04025*, 2015.
- [39] A. Vaswani, N. Shazeer, N. Parmar, J. Uszkoreit, L. Jones, A. N. Gomez, Ł. Kaiser, and I. Polosukhin, "Attention is all you need," *Advances in neural information processing systems*, vol. 30, 2017.
- [40] F. Mentzer, E. Agustsson, M. Tschannen, R. Timofte, and L. Van Gool, "Conditional probability models for deep image compression," in *Proceedings of the IEEE Conference on Computer Vision and Pattern Recognition*, 2018, pp. 4394–4402.
- [41] Y. Zhang, K. Li, K. Li, B. Zhong, and Y. Fu, "Residual non-local attention networks for image restoration," in *International Conference on Learning Representations*, 2019.
- [42] Z. Tang, H. Wang, X. Yi, Y. Zhang, S. Kwong, and C.-C. J. Kuo, "Joint graph attention and asymmetric convolutional neural network for deep image compression," *IEEE Transactions on Circuits and Systems for Video Technology*, vol. 33, no. 1, pp. 421–433, 2023.
- [43] Y. Qian, X. Sun, M. Lin, Z. Tan, and R. Jin, "Entroformer: A transformer-based entropy model for learned image compression," in *International Conference on Learning Representations*, 2022.
- [44] A. B. Koyuncu, H. Gao, A. Boev, G. Gaikov, E. Alshina, and E. Steinbach, "Contextformer: A transformer with spatio-channel attention for context modeling in learned image compression," in *Computer Vision–ECCV 2022: 17th European Conference, Tel Aviv, Israel, October 23–27, 2022, Proceedings, Part XIX*. Springer, 2022, pp. 447–463.
- [45] M. Jaderberg, K. Simonyan, A. Zisserman *et al.*, "Spatial transformer networks," *Advances in neural information processing systems*, vol. 28, 2015.
- [46] A. Recasens, P. Kellnhöfer, S. Stent, W. Matusik, and A. Torralba, "Learning to zoom: a saliency-based sampling layer for neural networks," in *Proceedings of the European Conference on Computer Vision (ECCV)*, 2018, pp. 51–66.
- [47] H. Talebi and P. Milanfar, "Learning to resize images for computer vision tasks," in *Proceedings of the IEEE/CVF International Conference on Computer Vision*, 2021, pp. 497–506.
- [48] D. Marin, Z. He, P. Vajda, P. Chatterjee, S. Tsai, F. Yang, and Y. Boykov, "Efficient segmentation: Learning downsampling near semantic boundaries," in *Proceedings of the IEEE/CVF International Conference on Computer Vision*, 2019, pp. 2131–2141.
- [49] C. Jin, R. Tanno, T. Mertzaniidou, E. Panagiotaki, and D. C. Alexander, "Learning to downsample for segmentation of ultra-high resolution images," in *International Conference on Learning Representations*, 2022.
- [50] L.-H. Chen, C. G. Bampis, Z. Li, L. Krasula, and A. C. Bovik, "Estimating the resize parameter in end-to-end learned image compression," *arXiv preprint arXiv:2204.12022*, 2022.
- [51] J. Ballé, V. Laparra, and E. P. Simoncelli, "End-to-end optimized image compression," in *International Conference on Learning Representations*, 2017.
- [52] T. Chen, H. Liu, Z. Ma, Q. Shen, X. Cao, and Y. Wang, "Neural image compression via non-local attention optimization and improved context modeling," *arXiv preprint arXiv:1910.06244*, 2019.
- [53] Kodak. (1999) Kodak test images. <http://r0k.us/graphics/kodak/>.
- [54] N. Asuni and A. Giachetti, "Testimages: a large-scale archive for testing visual devices and basic image processing algorithms."
- [55] JPEG-AI. (2020) Jpeg-ai test images. https://jpegai.github.io/test_images/.
- [56] C. 2022. (2022) 5th workshop and challenge on learned image compression. <http://compression.cc/tasks/>.
- [57] J. Ballé, S. J. Hwang, and E. Agustsson, "TensorFlow Compression: Learned data compression," 2022. [Online]. Available: <http://github.com/tensorflow/compression>
- [58] G. Bjontegaard, "Calculation of average psnr differences between rd-curves," *VCEG-M33*, 2001.
- [59] Y. Xie, K. L. Cheng, and Q. Chen, "Enhanced invertible encoding for learned image compression," in *Proceedings of the 29th ACM International Conference on Multimedia*, 2021, pp. 162–170.